Nucleic Acids Research, 2025, **53**, gkaf440
https://doi.org/10.1093/nar/gkaf440
Synthetic Biology and Bioengineering

Quantum-inspired logic for advanced Transcriptional Programming

Prasaad T. Milner, Dowan Kim, Corey J. Wilson

Georgia Institute of Technology, School of Chemical & Biomolecular Engineering, 311 Ferst Drive, Atlanta, GA 30332-0100, United States
*To whom correspondence should be addressed. Email: corey.wilson@chbe.gatech.edu

Abstract

The tenets of intelligent biological systems are (i) scalable decision-making, (ii) inheritable memory, and (iii) communication. This study aims to increase the complexity of decision-making operations beyond standard Boolean logic, while minimizing the metabolic burden imposed on the chassis cell. To this end, we present a new platform technology for constructing genetic circuits with multiple OUTPUT gene control using fewer INPUTs relative to conventional genetic circuits. Inspired by principles from quantum computing, we engineered synthetic bidirectional promoters, regulated by synthetic transcription factors, to construct 1-INPUT, 2-OUTPUT logical operations—i.e. biological QUBIT and PAULI-X logic gates—designed as compressed genetic circuits. We then layered said gates to engineer additional quantum-inspired logical operations of increasing complexity—e.g. FEYNMAN and TOFFOLI gates. In addition, we engineered a 2-INPUT, 4-OUTPUT quantum operation to showcase the capacity to utilize the entire permutation INPUT space. Finally, we developed a recombinase-based memory operation to remap the truth table between two disparate logic gates—i.e. converting a QUBIT operation to an antithetical PAULI-X operation *in situ*. This study introduces a novel and versatile synthetic biology toolkit, which expands the biocomputing capacity of Transcriptional Programming via the development of compressed and scalable multi-INPUT/OUTPUT logical operations.

Graphical abstract

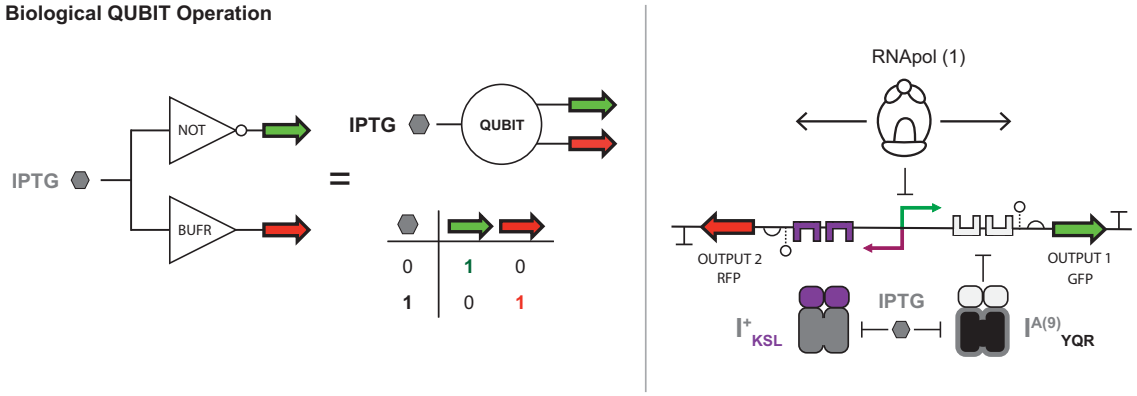

Introduction

Synthetic biologists have made large strides toward engineering intelligent biological systems using gene regulatory networks [1–8]. To date, synthetic biotic systems have drawn inspiration from classical computing, where sets of fundamental logical operations are engineered in single cells and modularly combined to create genetic circuits [2, 5, 9–14]. These programs have shown great promise in biomanufacturing [15–17], metabolic engineering [18–20], biocontainment [21–23], agriculture [24–26], and therapeutic [27–30] applications. However, as the application space for synthetic biological programs expands, there is a growing need for more resource efficient biological programming structures that enable an increase in circuit complexity to better meet point-of-use functionality [31].

One way to achieve greater programming efficiency is via circuit compression—i.e. reducing the number of parts used to construct a given genetic circuit or genetic operation. To this end, Transcriptional Programming (T-Pro) has emerged as the state of the art regarding circuit compression [9, 10, 13]. T-Pro leverages modular sets of synthetic transcription factors and cognate synthetic promoters to achieve circuit compression via networked functions. A fundamental advantage of this toolkit is the use of two classes of synthetic transcription factors: (i) repressors and (ii) anti-repressors—which can be abstracted to BUFFER and NOT logic gates, respectively.

Received: October 14, 2024. **Revised:** April 27, 2025. **Editorial Decision:** May 3, 2025. **Accepted:** May 12, 2025

When repressors and anti-repressors are employed to regulate a user-defined genetic architecture composed of cognate synthetic promoters, T-Pro can form complete sets of compressed Boolean logical operations—analogous to the fundamental decision-making units of a computer program.

We posit that T-Pro can be extended beyond standard Boolean logic to emulate information transfer observed in quantum computing systems [32–34]. A key advantage of quantum programming is logical reversibility, wherein each OUTPUT state can be mapped to a specific INPUT state and vice versa—a distinguishing feature relative to classical bit (binary) programming. Quantum computing reversible logic should not be conflated with thermodynamic reversibility—see Supplementary Note S1. Quantum computing is not necessarily quantum mechanical, rather said computing leverages and emulates an abstraction of reversible logical operations in the form of QUBITs where a system can represent not just one possibility, but multiple possibilities—commonly referred to as a superposition. In this study, our objective is to design analogous quantum logical operations in the context of biological circuits. Namely, we aim to design a fundamental biological QUBIT logical operation in which each INPUT state maps to a unique dual-state OUTPUT—i.e. where the OUTPUT vector is $|0\rangle$ = [1,0] when the INPUT is 0, and is $|1\rangle$ = [0,1] when the INPUT is 1 (see Fig. 1A–C). Ideally, the resulting biological QUBIT can be entangled with other biological unit operations—i.e. in the sense that multiple quantum operations can be correlated with a high probability, enabling the systematic development of multi-INPUT multi-OUTPUT biological programs with more efficient INPUT economy (Supplementary Fig. S1 and Supplementary Note S1).

In quantum computing systems, reversible logic is utilized to reduce calculation cost (i.e. the number of gates used to construct a program) and the number of OUTPUT states that are not the primary OUTPUT or that advance the computation [33, 34]. In practice, programs predicated on quantum reversible logic can modulate two or more OUTPUTs with fewer INPUTs compared to classical systems. Axiomatically, fundamental units of reversible logic can be layered (or entangled) to form operations of higher complexity. In principle, quantum (reversible) logic applied to biological systems has the potential to dramatically reduce the number of genetic parts required for a given circuit—analogous to abiotic systems. Said technology could be used in multi-product biomanufacturing, branched-pathway metabolic engineering applications, or any nonlinear multistep biological process wherein multiple OUTPUT regulation benefits from efficient INPUT economy.

Many reversible logic gates have been developed abiotically using superconducting devices [35], via optics [36, 37], enzymatically [38, 39], and recently in living systems by way of a community-level platform [40, 41]. However, the biological (biotic) iterations of said logic gates do not operate at a single-cell level and require a population to measure, which is prone to instability due to community-level fluctuation. To our knowledge, only one example of a single-cell reversible gate has been reported [42]. This system is constructed with two duplicate GFP OUTPUTs to achieve an apparent FEYNMAN gate truth table; therefore, the operation cannot be technically classified as a reversible gate regarding the true transcriptional OUTPUTs. To facilitate open-ended synthesis of efficient and complex genetic circuits, a modular platform for constructing reversible logic is needed. We posit that T-Pro can serve as a platform technology for this purpose.

In this work, we present novel T-Pro biocomputing circuits inspired by quantum computing principles using *Escherichia coli* as the chassis cell. Said technology is achieved via (i) engineering novel synthetic bidirectional promoters that facilitate transcription of a dual-state OUTPUT and (ii) developing single-INPUT transcriptional control of the OUTPUT state via complementary synthetic repressor and anti-repressor transcription factors from the T-Pro toolkit. In this study, we demonstrated that our platform is modular and scalable from 1-INPUT operations to 2-INPUT and 3-INPUT reversible logic programs. Commensurate with our supposition, said operations increased information transfer in genetic circuits by purposing a greater portion of the INPUT permutation space for reversible logic OUTPUTs. Furthermore, we demonstrated that our new platform technology seamlessly pairs with our complementary memory operations [43, 44]—demonstrated as truth table remapping between two fundamental quantum operations *in situ*. This platform technology represents a paradigm shift in biocomputing, advancing the current state of genetic programming technology by enabling and expansion of efficient computation in carbon that leverages the systemization of T-Pro.

Materials and methods

Cloning, strains, and media

Transcription factors and recombinases were expressed on the pLacI plasmid (Novagen) that contains the p15a origin (copy number 20–30/cell) and output genes (GFP = sfGFP, RFP = mCherry, BFP (blue fluorescent protein) = tagBFP, YFP (yellow fluorescent protein) = phiYFP) were expressed on the pZS*22-sfGFP reporter plasmid that contains the pSC101 origin (copy number 3–5/cell). Chloramphenicol and kanamycin resistance genes were used as selection markers for transcription factor and reporter plasmids, respectively. Output genes were assembled into reporter plasmids using Golden Gate Assembly (BsaI-HF v2 Golden Gate Assembly Kit, NEB). Transcription factors were first subcloned into pUC19 vector carrying an ampicillin resistance gene (NEB) with BsmBI restriction sites, grown in LB with carbenicillin, sequence confirmed with Sanger DNA sequencing (Eurofins Genomics), and then assembled into the pLacI plasmid using Golden Gate Assembly (BsmBI-HF v2 Golden Gate Assembly Kit, NEB). A pLacI destination plasmid with PhlF and A118 was constructed using Gibson Assembly (NEBuilder HiFi DNA Assembly Master Mix, NEB) for generating the memory transcription factor plasmids. All promoter, operator, insulator, RBS (ribosome binding site), and terminator sequences were cloned using site-directed mutagenesis polymerase chain reaction (Q5 DNA Polymerase, NEB) with custom primers (Eurofins Genomics) followed by kinase, ligase, and DpnI reactions (KLD enzyme mix, NEB) prior to final construct assemblies. All genetic parts used in transcriptional logic gates can be found in Supplementary Figs S2–S5. All promoter, operator, insulator, RBS, terminator, and coding sequences can be found in Supplementary Tables S1–S6. All cloning plasmids in this work were transformed into chemically competent DH5α cells [huA2 Δ (argF-lacZ)U169 phoA glnV44 φ80Δ (lacZ)M15 gyrA96 recA1 relA1 endA1 thi-1 hsdR17; New England Biolabs] and plated on LB agar with appropriate antibiotics. Resulting transformants were cultured overnight in LB broth with appropriate antibiotics and miniprepped (Omega Bio-Tek) to yield each plasmid, and sequence was

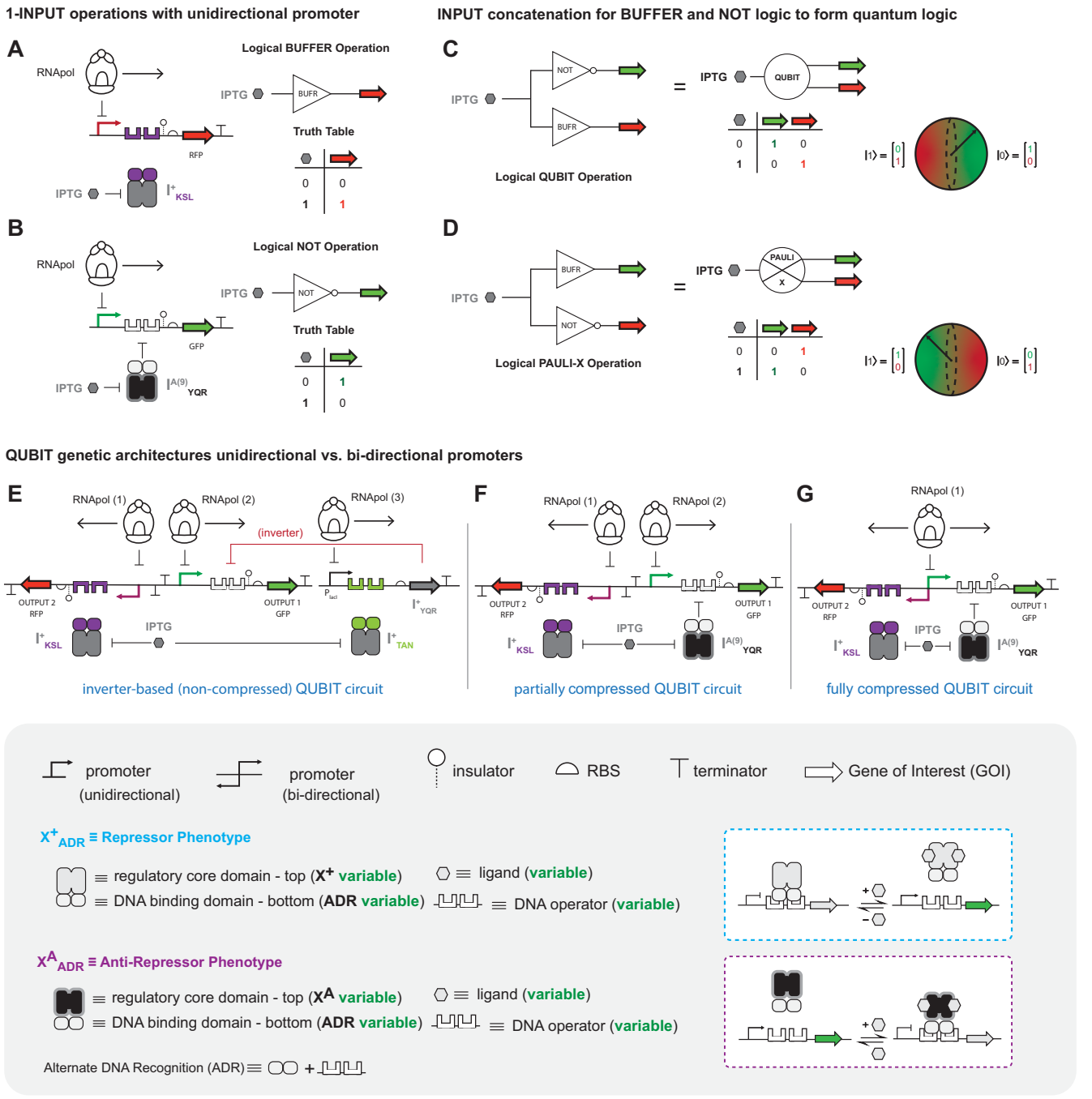

Figure 1. Design of a fully compressed biological QUBIT logic operation. (**A**, **B**) Complementary logical operations for developing biological QUBIT logic. The biological QUBIT gate is comprised of (i) a logical BUFFER operation with the synthetic LacI transcription factor I^{+}_{KSL} regulating the OUTPUT RFP (red fluorescent protein) in panel (A) and (ii) a logical NOT operation with the synthetic anti-LacI transcription factor $I^{A(9)}_{YQR}$ regulating the OUTPUT GFP (green fluorescent protein). Gate diagrams, genetic architectures, and truth tables are shown. (**C**) Gate diagrams showing concatenation of BUFFER and NOT logic operations via INPUT coupling (i.e. combination of both operations in a single cell) to perform biological QUBIT logic. (**D**) Gate diagrams showing concatenation of BUFFER and NOT logic operations via INPUT coupling to perform biological PAULI-X logic (i.e. antithetical to the QUBIT operation). (E, F) Genetic architecture designs for biological QUBIT logic. (**E**) An inverter-based QUBIT circuit, (**F**) a partially compressed QUBIT circuit that utilizes an anti-repressor to eliminate the inverter, and (**G**) a fully compressed QUBIT circuit that leverages an anti-repressor and a bidirectional promoter. The inverter-based QUBIT requires the most resources, 3 RNA polymerases + 3 transcription factors. The partially compressed QUBIT requires fewer resources, 2 RNA polymerases + 2 transcription factors. Notably, the fully compressed iteration of the QUBIT operation requires the fewest number of resources, 1 RNA polymerase + 2 transcription factors. The design of the fully compressed QUBIT is composed of a single bidirectional promoter driving the transcription of GFP and RFP, which are each regulated as described in panels (A) and (B)—both transcription factors recognize a single INPUT [i.e. isopropyl-β-D-thiogalactoside (IPTG)], yet perform opposite regulatory phenotypes upon induction. Legend describes the iconography used in the circuit designs.

confirmed with NGS Whole Plasmid DNA sequencing (Eurofins Genomics).

Transcriptional logic gate experiments

Transcription factor and corresponding reporter plasmids were double transformed into homemade chemically competent 3.32 *E. coli* cells [Genotype lacZ13 (Oc), lacI22, LAM−, el4−, relA1, spoT1, and thiE1, Yale CGSC #5237] and six individual transformants (biological replicates) were precultured for 6 h in LB media with chloramphenicol (25 μg/ml, VWR Life Sciences) and kanamycin (35 μg/ml, VWR Life Sciences) antibiotics. Precultures were then diluted into glucose (100 mM, Fisher Scientific) M9 minimal media supplemented with 0.2% (w/v) casamino acids (VWR Life Sciences), 1 mM thiamine HCl (Alfa Aesar), antibiotics, and respective inducers, and grown in a flat-bottom 96-well microplate (Costar) for 16 h (37°C, 300 rpm). Microwell plates were sealed with Breathe-Easy membranes (Diversified Biotech) to prevent evaporation. Inducer concentrations used are as follows: IPTG (10 mM), D-ribose (10 mM), and cellobiose (10 mM). Optical density (OD_{600}), GFP fluorescence (λ_{ex} = 485 nm, λ_{em} = 510 nm, Gain 400), RFP fluorescence (λ_{ex} = 585 nm, λ_{em} = 610 nm, Gain 800), BFP fluorescence (λ_{ex} = 399 nm, λ_{em} = 454 nm, Gain 400), and YFP fluorescence (λ_{ex} = 517 nm, λ_{em} = 557 nm, Gain 400) were measured with a Spectramax M2e plate reader (Molecular Devices). The LacSTOP control plasmid was also assayed with each reporter construct to determine the maximum expression level of each genetic architecture. Measurements were corrected by subtracting values of blank media from sample values and fluorescence values were normalized to optical density in Microsoft Excel (Microsoft) and divided by a global maximum (per fluorescent channel) to obtain the fraction of maximum output. For 1-INPUT and 2-INPUT gate plots with a single *y*-axis scale, fluorescence values were divided by the 2-OUTPUT reporter maximum of 15 000 relative fluorescence units (RFU) for GFP and 300 RFU for RFP. A built-in log(agonist) versus normalized response model in GraphPad (Prism) was used to fit experimental dose response data, and fitting parameters are given in Supplementary Data. For the 3-INPUT TOFFOLI gate, fluorescence values were divided by the 3-OUTPUT reporter maximum of 6000 RFU for GFP, 200 RFU for RFP, and 2500 RFU for BFP. For the 4-OUTPUT gate, fluorescence values were divided by the reporter maximum of 1500 RFU for GFP, 100 RFU for RFP, 1500 RFU for BFP, and 1500 RFU for YFP. Resulting data were plotted using GraphPad (Prism).

Library generation and screening

Promoter and RBS libraries were generated using site-directed mutagenesis as described above with primers containing N (A, T, C, or G), R (A or G), or S (G or C) nucleotides (Eurofins Genomics) to constitute the resulting library space. Library mutagenesis reactions were performed on individual transcription factors subcloned in pUC19 and transformed in chemically competent DH5*α* cells as descried above. The recovery was outgrown in LB with carbenicillin overnight and miniprepped. The resulting DNA library subclones were subsequently used in Golden Gate Assemblies to generate IR (IPTG–D-ribose) FEYNMAN, RI FEYNMAN, and EIR TOFFOLI gate libraries. Following assembly, libraries were transformed, dilution plated (to calculate library size), outgrown in LB with chloramphenicol, and miniprepped. The assembled DNA libraries were then double transformed with corresponding reporter plasmids into 3.32 *E. coli* as described above. Individual colonies were picked for screening and assayed. The top 7 performing clones were then streaked onto LB agar with chloramphenicol and kanamycin antibiotics and re-assayed with six biological replicates as described previously. Top-performing variants were then grown in LB with antibiotics, miniprepped, and sequenced.

Memory (recombinase) experiments

Circuit plasmids containing A118 regulated by PhlF and either IPTG or D-ribose inducible transcription factors (see Supplementary Fig. S5) were transformed into 3.32 *E. coli* cells and plated on LB agar with 25 μg/ml chloramphenicol. A transformant containing each type of memory plasmid (i.e. IPTG QUBIT, IPTG PAULI-X, D-ribose QUBIT, or D-ribose PAULI-X) was cultured in LB with antibiotics and used to generate chemically competent cells. Resulting competent cells were transformed with the memory reporter plasmid that contains A118 attachment sites, and six transformants (biological replicates) were precultured for 6 h in LB media with chloramphenicol and kanamycin antibiotics. Precultures were diluted into glucose M9 minimal media and assayed as described above. Assay cultures were then diluted 1:100 into (i) phosphate buffered saline (PBS) containing 10× kanamycin (350 μg/ml) for flow cytometry analysis and (ii) fresh LB media containing 10 μM 2,4-diacetylphophloroglucinol (DAPG) and appropriate antibiotics. Cultures were grown in 96-well microplate (37°C, 300 rpm) sealed with a Breathe-Easy membrane (Diversified Biotech) for 8 h to allow for recombination. Cultures were then diluted into glucose M9 minimal media with appropriate inducer conditions and assayed again as described above. Assay cultures were diluted into PBS for flow cytometry analysis.

Flow cytometry

Flow cytometry analysis was performed with a Cytoflex S (Beckman Coulter) flow cytometer. After the memory (recombinase-based) experiments, cells were diluted 1:40 into PBS with 2 mg/ml of kanamycin and incubated for an hour at room temperature. Cells were then analyzed at 20–30 μl/min flow rate and gated by forward scatter versus side scatter (SSC) to eliminate cell debris. To gate the correct cell population, events were further gated by SSC height versus SSC area. Fluorescence was monitored through the FITC channel for GFP expression and ECD channel for RFP expression. More than 20 000 events were collected and analyzed by CytExpert (Version 2.5) software. All flow cytometry assays had six biological replicates. A representative gating strategy is described in Supplementary Fig. S6.

Results

Engineering a 2-OUTPUT synthetic promoter for QUBIT logic

Inspired by the function of the QUBIT operation used in quantum computing—in which a single INPUT maps to two OUTPUTs—we posited that we could engineer a genetic analog leveraging T-Pro synthetic transcription factors and cognate genetic elements. To accomplish this, first we constructed two fundamental T-Pro operations: (i) a logical BUFFER operation using the synthetic transcription factor I^{+}_{KSL} [9]

(repressor) mapped to the regulation of RFP (Fig. 1A) and (ii) an antithetical logical NOT operation via the synthetic transcription factor $I^{A(9)}{}_{YQR}$ [10, 45] (anti-repressor) mapped to the regulation of GFP (Fig. 1B). Notably, both synthetic transcription factors respond to the same INPUT—IPTG—with orthogonal DNA-binding functions. We posited that we could design a biological QUBIT logical operation (Fig. 1C)—and in turn an antithetical PAULI-X operation (Fig. 1D) using similar design rules—in which a 1-INPUT inducible system modulates two disparate OUTPUTs. We posited that the QUBIT design goal shown in Fig. 1C could be accomplished via three disparate genetic circuits: (i) an inverter-based QUBIT circuit (Fig. 1E), (ii) a partially compressed QUBIT circuit that utilizes an anti-repressor to eliminate the inverter (Fig. 1F), or (iii) a fully compressed QUBIT circuit that leverages an anti-repressor and a bidirectional promoter (Fig. 1G). Prominently, all designs required the use of T-Pro synthetic transcription factors to facilitate single INPUT control over multiple OUTPUTs. The inverter-based QUBIT requires the most resources, 3 RNA polymerases + 3 transcription factors. The partially compressed QUBIT requires fewer resources, 2 RNA polymerases + 2 transcription factors. Notably, the fully compressed iteration of the QUBIT operation requires the fewest number of resources, 1 RNA polymerase + 2 transcription factors. The use of two separate promoters would result in uncoupled transcription of the OUTPUTs due to independent RNA polymerase binding events (Fig. 1F). Accordingly, we opted for a bidirectional promoter design that yields divergent transcription from a single RNA polymerase binding locus (Fig. 1G), and in principle will impose the smallest metabolic burden on the chassis cell. Although not commonly used in genetic circuits, bidirectional promoters have recently been found to comprise 19% of all detected transcriptional start sites in *E. coli* as well as play an important role in gene co-regulation regulation [46]; thus, our design goal given in Fig. 1G is plausible. As designed, our putative genetic QUBIT couples the expression of two OUTPUT states—GFP or RFP production—to the initiation of a single information transfer event.

To achieve the fully compressed QUBIT design given in Fig. 1G, we engineered three iterations of synthetic bidirectional promoters designed using pTrc and pJ23119 promoter sequences driving GFP and RFP OUTPUTs, respectively (Fig. 2A). Namely, we systematically varied the placement of promoter elements to construct three overlapping and symmetric putative bidirectional promoter configurations: (i) $P^{BD(10)}{}_{rep}$—convergent orientation with a single −10 hexamer, (ii) $P^{BD(17)}{}_{rep}$—divergent orientation with overlapping spacer regions, and (iii) $P^{BD(35)}{}_{rep}$—divergent orientation with a single −35 hexamer. Additionally, we built a reporter with independent unidirectional promoters as a control. To complete the design of the synthetic bidirectional promoters, we incorporated tandem O^{agg} and O^{sym} synthetic operators—corresponding to cognate synthetic transcription factors $I^{+}{}_{KSL}$ (repressor) and $I^{A(9)}{}_{YQR}$ (anti-repressor)—to facilitate discrete regulation of RFP and GFP, respectively. In addition, we included genetic insulators downstream of each hexamer set to normalize the production of each messenger RNA transcript (see Fig. 2A and Supplementary Figs S2, S7, and S8).

Next, we experimentally tested each QUBIT synthetic promoter using single synthetic transcription factors to evaluate discrete INPUT to OUTPUT performance. Our results indicated that the $P^{BD(35)}{}_{rep}$ synthetic promoter performed the best in the context of discrete regulation of GFP and RFP (Fig. 2B and Supplementary Fig. S8). We speculated that the $P^{BD(10)}{}_{rep}$ configuration exhibited poor regulatory performance due to off-target distal regulation resulting from operator proximity to the −35 hexamers, evidenced by significant changes in expression of the unregulated GFP and RFP channels upon induction. In addition, we observed that the $P^{BD(10)}{}_{rep}$ design demonstrated low GFP expression and greater leakiness in RFP regulation compared to $P^{BD(35)}{}_{rep}$. To evaluate whether the engineered $P^{BD(35)}{}_{rep}$ synthetic promoter has the capacity to reduce cellular resource competition (i.e. endogenous RNA polymerase sequestering [47]; also see comment given in Supplementary Fig. S7) compared to the two independent promoter configuration, we conducted an experiment analogous to the above using a ribose-inducible repressor–anti-repressor pair with the inclusion of an additional plasmid to simulate cellular burden, and measured the change in OUTPUT upon inducer titration (Supplementary Fig. S9). We observed that for both configurations, the OUTPUT of each unregulated channel (i.e. GFP expression when only $R^{+}{}_{KSL}$ is present, and RFP expression when only $R^{A(2)}{}_{YQR}$ is present) decreased as the opposing regulated channel was induced—implying a putative cellular resource competition. Moreover, the magnitude of this effect was lower with $P^{BD(35)}{}_{rep}$ compared to the independent promoter configuration, indicating that $P^{BD(35)}{}_{rep}$ provided an advantage with regard to mitigating cellular resource competition compared to conventional promoter designs in genetic circuits. Accordingly, we selected the $P^{BD(35)}{}_{rep}$ synthetic promoter configuration for all logical operations developed herein.

Building and testing a fully compressed biological QUBIT operation

Following the characterization of the discrete INPUT to OUTPUT performance of the $P^{BD(35)}{}_{rep}$ synthetic promoter, we tested the said bidirectional promoter in the presence of co-expressed $I^{+}{}_{KSL}$ (repressor) and $I^{A(9)}{}_{YQR}$ (anti-repressor)—with and without the cognate INPUT (IPTG). Qualitatively, we observed the correct QUBIT phenotype (Fig. 2C). However, this first iteration QUBIT operation exhibited a significant reduction in regulatory performance relative to the single INPUT biosensor systems given in Supplementary Fig. S8—particularly in the GFP anti-repression channel. Given that both synthetic transcription factors function as homotetramers—with homodimers as the fundamental functional unit—we posited that $I^{+}{}_{KSL}$ and $I^{A(9)}{}_{YQR}$ monomers formed nonfunctional heterodimers stabilized by the tetramerization domain (see Fig. 2C, inset).

To resolve the obfuscated function between the repressor and anti-repressor in the context of the QUBIT operation, we first introduced an L251A mutation at the monomer–monomer interface of the $I^{+}{}_{KSL}$ repressor. The said mutation in wild-type LacI restricts assembly and function to the tetrameric form of the protein [48]. In addition, we truncated 12 residues from the C-terminus of the $I^{A(9)}{}_{YQR}$ anti-repressor. This modification in wild-type LacI prevents tetramerization while maintaining the assembly of functional dimers [49]. In principle, the mutated repressor can only function as a tetramer, and the truncated anti-repressor is restricted to dimer formation. We posited that this set of modifications should eliminate heterodimer and heterotetramer formation—i.e. biasing function to exclusive homogeneous

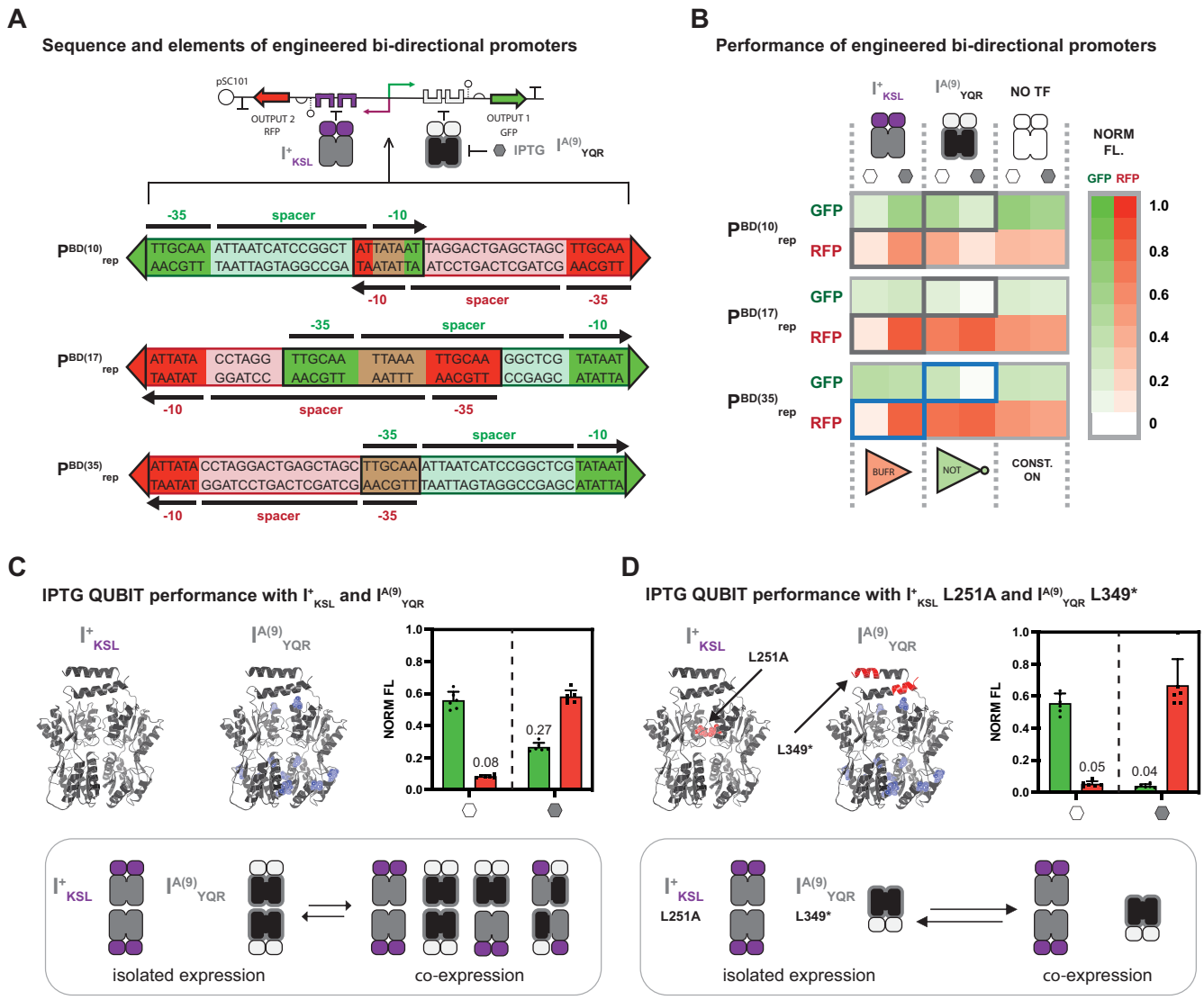

Figure 2. Bidirectional promoter architectures and regulatory performance. (**A**) DNA elements of engineered bidirectional promoters. Green regions represent promoter elements driving GFP expression, and red regions represent promoter elements driving RFP expression. Brown regions represent promoter elements driving both GFP and RFP expression. (**B**) Regulatory performance of each bidirectional promoter with (i) IPTG BUFFER logic via I^{+}_{KSL} regulation of RFP, (ii) IPTG NOT logic via $I^{A(9)}_{YQR}$ regulation of GFP, or (iii) constitutive expression with no transcription factor. Each box represents a GFP or RFP OUTPUT value for each promoter configuration, regulatory element, and ligand state. (**C**) Crystal structure of wild-type LacI tetramer (PDB: 1LBI), which is used as a visual representation of I^{+}_{KSL} and $I^{A(9)}_{YQR}$ transcription factors, with mutations conferring the $I^{A(9)}_{YQR}$ phenotype highlighted in dark blue. Performance of the IPTG biological QUBIT logical operation (C, D). Both I^{+}_{KSL} and $I^{A(9)}_{YQR}$ were co-expressed and regulate the 2-OUTPUT reporter system with the $P^{BD(35)}_{rep}$ promoter configuration. (C) Note the OFF state of GFP is considerably leakier than the system in panel (B) with $I^{A(9)}_{YQR}$ only. (**D**) Crystal structures shown in panel (C) with I^{+}_{KSL} L251A and $I^{A(9)}_{YQR}$ L349* mutations highlighted in red, and performance of IPTG biological QUBIT with I^{+}_{KSL} L251A and $I^{A(9)}_{YQR}$ L349* to restrict heterotetrametric and heterodimeric protein assemblies. The GFP and RFP OFF states decreased by 6.75× and 1.6× from those in panel (C), respectively. In all experiments, GFP and RFP OUTPUT fluorescence measurements were normalized to maximum values of 15 000 RFU and 300 RFU, respectively, and are shown here on a fractional scale (also see the "Materials and methods" section). Crystal structure images were generated using 3D Protein Imaging [58].

functional assemblies during co-expression (Fig. 2D), resulting in a significant improvement in QUBIT performance. Consistent with our supposition, we observed a marked increase in performance upon modification of both synthetic transcription factors (Figs 2D and 3A).

Next, we constructed D-ribose inducible (Fig. 3B) and fructose inducible (Supplementary Fig. S10) biological QUBIT gates analogous to the IPTG operation described above. Unlike the IPTG system, said operations did not require additional modifications to achieve the desired performance (also see Supplementary Note S2). In summary, all biological unit operations (i.e. IPTG, D-ribose, and fructose inducible systems) demonstrated logic congruent with QUBIT gates used in quantum computing, where the OUTPUT vector [GFP, RFP] is $|0\rangle = [1,0]$ when the INPUT (ligand) is 0, and is $|1\rangle = [0,1]$ when the INPUT is 1. Furthermore, each gate exhibited a dose-dependent OUTPUT wherein fractional states of each OUTPUT between the values of 0 and 1 are possible, which is analogous to the properties of QUBITs used in quantum computing. Additionally, our quantum-inspired T-Pro technology can accommodate the regulation of coding and noncoding RNA. To illustrate the latter iteration we designed, built, and tested

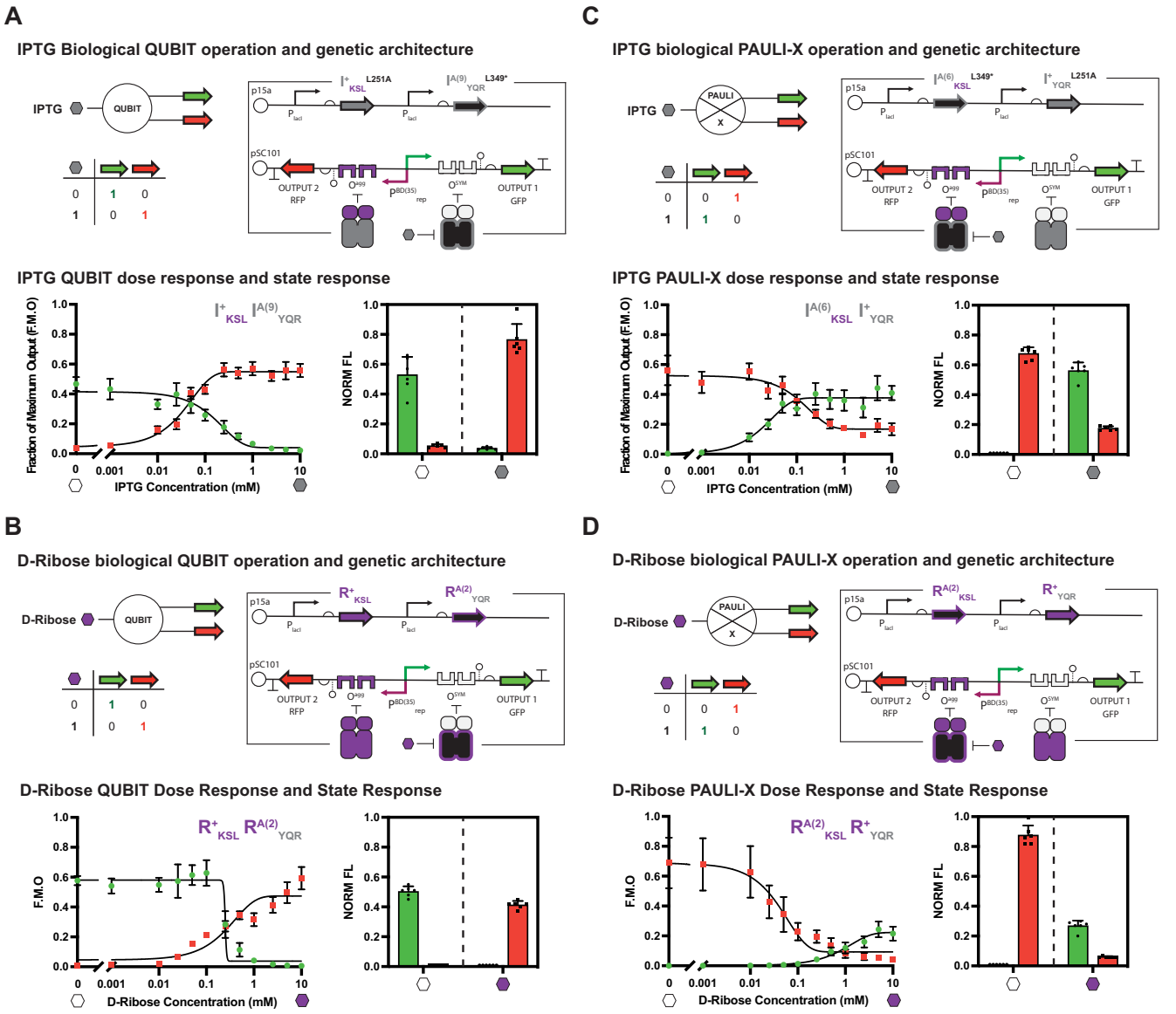

Figure 3. Biological QUBIT and PAULI-X logic gates. Gate diagram, truth table, genetic architecture, dose response, and state response of (**A**) IPTG biological QUBIT logical operation employing I^{+}_{KSL} L251A and $I^{A(9)}_{YQR}$ L349* transcription factors; (**B**) D-ribose biological QUBIT logical operation employing R^{+}_{KSL} and $R^{A(2)}_{YQR}$ transcription factors; (**C**) IPTG biological PAULI-X logical operation employing $I^{A(6)}_{KSL}$ L349* and I^{+}_{YQR} L251A transcription factors; and (**D**) D-ribose biological PAULI-X logical operation employing $R^{A(2)}_{KSL}$ and R^{+}_{YQR} transcription factors. The 2-OUTPUT reporter with the $P^{BD(35)}_{rep}$ promoter configuration was used for all logic gates. Data are representative of six biological replicates per experiment. Dose response and state response data were obtained with separate experiments on different days. Dose response data were fit with a Hill function curve (parameters and statistics are given in Supplementary Data).

a CRISPRi QUBIT operation (see Supplementary Fig. S11). This development expands the utility of our platform technology, and in principle QUBIT operations can be used with any RNA-based technology that benefits from regulation in the context of a 1 INPUT, 2 OUTPUT operation.

Designing, building, and testing fully compressed biological PAULI-X operations

In quantum information theory, the PAULI-X logical operator performs a bit-flip relative to a QUBIT operation resulting in an antithetical truth table [50]; see relative abstractions given in Fig. 1C and D. In other words, the PAULI-X gate is the quantum equivalent of the NOT gate for classical binary computation. We posited that we could engineer a biological analogue of the PAULI-X logical operation using a similar design workflow to that developed for the biological QUBIT operations. The design of a biological PAULI-X logical operation leveraged the $P^{BD(35)}_{rep}$ synthetic promoter developed for the QUBIT operation (see Fig. 2A). Next, we selected two new synthetic transcription factors antithetical in phenotype—while preserving the mapped orthogonal DNA-binding functions—to the set used for the original QUBIT operation. Namely, we selected (i) the I^{+}_{YQR} repressor, opposed to the $I^{A(9)}_{YQR}$ anti-repressor, and (ii) the $I^{A(6)}_{KSL}$ anti-repressor, instead of the I^{+}_{KSL} repressor. Both synthetic transcription factors respond to the same INPUT (IPTG), with orthogonal DNA-binding functions. In addition, we carried over the mutations used in the previous section to prevent heterogeneous protein assemblies. In principle, the new set of

synthetic T-Pro transcription factors will invert the INPUT to OUTPUT truth table, relative to the corresponding QUBIT operation. Objectively, said remapping of the protein DNA interactions should result in the desired PAULI-X logical operation (see Fig. 3C). We tested the biological PAULI-X operation, and as expected, the circuit exhibited faithful qualitative performance.

Next, we developed a second PAULI-X operation responsive to the INPUT D-ribose (see Fig. 3D). As with the previous design, we used the $P^{BD(35)}{}_{rep}$ synthetic promoter paired with synthetic transcription factors complementary to the set used in the corresponding QUBIT operation given in Fig. 3B. Upon testing the operation, our second iteration PAULI-X logic gate resulted in the correct qualitative performance—consistent with our general design goal. The ability to confer PAULI-X logic with our system demonstrates that our programming structure retains important features of our T-Pro toolkit, which allows for systematic building—i.e. repurposing the synthetic bidirectional promoter—while maintaining circuit compression [10, 13]. In addition, we posited that QUBIT and PAULI-X operations can be leveraged to systematically engineer advanced biological programs of greater complexity with multi-OUTPUT decision-making.

Programming 2-INPUT FEYNMAN (CNOT) logic

In principle, we can systematically construct advanced reversible logic operations via modularly layering 1-INPUT units—i.e. implementing FEEDFORWARD functions. To demonstrate our ability to construct advanced quantum biocomputing operations via stacking QUBITs, we designed a FEYNMAN (controlled-NOT, or CNOT) gate, which is the equivalent of a reversible XOR gate, using two layered QUBIT gates. When combined with QUBITs, FEYNMAN gates are particularly useful in quantum computation as they constitute a universal logic set for simulating any quantum computing circuit. A FEYNMAN gate is a 2-QUBIT operation where the first (control) QUBIT flips the second (target) QUBIT only if the control QUBIT is $|1\rangle$ (Fig. 4A and B). Our design started with an IPTG-inducible control QUBIT layer, which regulated $R^{A(2)}{}_{KSL}$ (anti-repressor) and $R^{+}{}_{KSL}$ (repressor) OUTPUTs—such that (i) an INPUT of 0 maps to $R^{+}{}_{KSL}$ (repressor) OUTPUT and (ii) an INPUT of 1 maps to $R^{A(2)}{}_{KSL}$ (anti-repressor) OUTPUT. The D-ribose-inducible OUTPUTs (i.e. synthetic transcription factors) from layer one map to a second QUBIT layer—i.e. the unit operation given in Fig. 3B—such that the terminal layer regulates a set of observable OUTPUTs (see Fig. 4B).

On the first layer, we engineered a bidirectional promoter analogous to the $P^{BD(35)}{}_{rep}$ promoter to drive the expression of two transcription factors with a similar level to the individual p^{LacI} promoter while retaining our platform's architectural design. To accomplish this, we created a small promoter library (1024 variants) on the 17 bp spacer region driving $R^{+}{}_{KSL}$ transcription to reduce promoter secondary structure and tune expression, as well as an RBS/start codon library (64 variants) for the $R^{+}{}_{KSL}$ OUTPUT to optimize circuit performance (Supplementary Fig. S12). Additionally, we used the phl2 RBS [2] on $I^{A(9)}{}_{HQN}$ to achieve tighter regulation. Following assembly and phenotypic screening of each library—examples given in Supplementary Fig. S13—we generated a variant that displays qualitative FEYNMAN gate logic (Fig. 4C). Next, we designed an analogous FEYNMAN gate with the reverse INPUT configuration—i.e. a D-ribose–IPTG inducible system (Supplementary Fig. S14A–C). In this design, we leveraged the same genetic architecture used in the IPTG–D-ribose system; however, we swapped the transcription factor regulatory core domains that are responsible for INPUT processing. This result demonstrated the scalability of our QUBIT programming system in the context of FEEDFORWARD operations, which is congruent with our design goal. We posited that the construction of a FEYNMAN gate via alternate strategies would require additional parts (specifically promoters) relative to the design presented in Fig. 4B. To illustrate the aforesaid, a summary of alternate FEYNMAN designs is given in Supplementary Fig. S14D. Briefly, an inverter-based (Cello) design requires nine inducible promoters; the apparent FEYNMAN gate designed by Srivastava *et al.* [42] requires four inducible promoters. However, our fully compressed design given in Fig. 4B only requires two inducible promoters (assuming a bidirectional promoter = 1 promoter, which is reasonable given that said promoter can only initiate a single information transfer event). We posit that this precept will hold for any circuit design that leverages fully compressed QUBIT/PAULI-X operations as fundamental building blocks.

Engineering 3-INPUT TOFFOLI (CCNOT) logic via gate layering

To further demonstrate our platform's layering capability, we engineered a 3-INPUT, 3-OUTPUT TOFFOLI (controlled-controlled-NOT, or CCNOT) gate by adding a third layer (i.e. an additional control layer) to the IPTG–D-ribose FEYNMAN gate discussed in the previous section. The TOFFOLI gate is a universal reversible logic gate (meaning that any circuit can be constructed from TOFFOLI gates) that inverts the state of a target QUBIT depending on the state of two control QUBITs [51] (Fig. 4D and E). In our design, we moved the constitutively expressed $I^{+}{}_{YQR}{}^{L251A}$ and $I^{A(9)}{}_{HQN}{}^{L349*}$ regulators used in the FEYNMAN gate to a third layer, which is regulated by the synthetic cellobiose repressor $E^{+}{}_{TAN}$. $E^{+}{}_{TAN}$ is expressed constitutively and directly regulates BFP, which was inserted into the reporter downstream of GFP as the control OUTPUT. Additionally, we added a copy of O^{tta}, the cognate operator to $E^{+}{}_{TAN}$, on the second layer regulating $R^{A(2)}{}_{KSL}$ to achieve the desired gate operation. Here, cellobiose and IPTG regulated the control layers 1 and 2, respectively, which modulated expression of D-ribose-inducible transcription factors and the state of the target layer (i.e. the combined OUTPUT state) (Fig. 4E). As with the construction of the FEYNMAN gate, we created and screened independent libraries comprised of 64 variable $E^{+}{}_{TAN}$ and 64 variable $R^{+}{}_{KSL}$ RBS/start codon sequences to optimize regulatory performance. From our screen, we identified a variant with the desired TOFFOLI gate performance (Fig. 4F). This result reinforces our supposition regarding the modularity and expandability of our quantum logic T-Pro structure in the context of FEEDFORWARD operations.

Engineering biological QUBIT logic to modulate four OUTPUTs via two INPUTs

To demonstrate the utility of our engineered biological QUBIT gates in genetic circuit design, we built a 4-OUTPUT circuit modulated by two discrete INPUTs—IPTG and D-ribose. This circuit can activate each OUTPUT individually via a unique INPUT permutation, thereby utilizing 100% of the INPUT

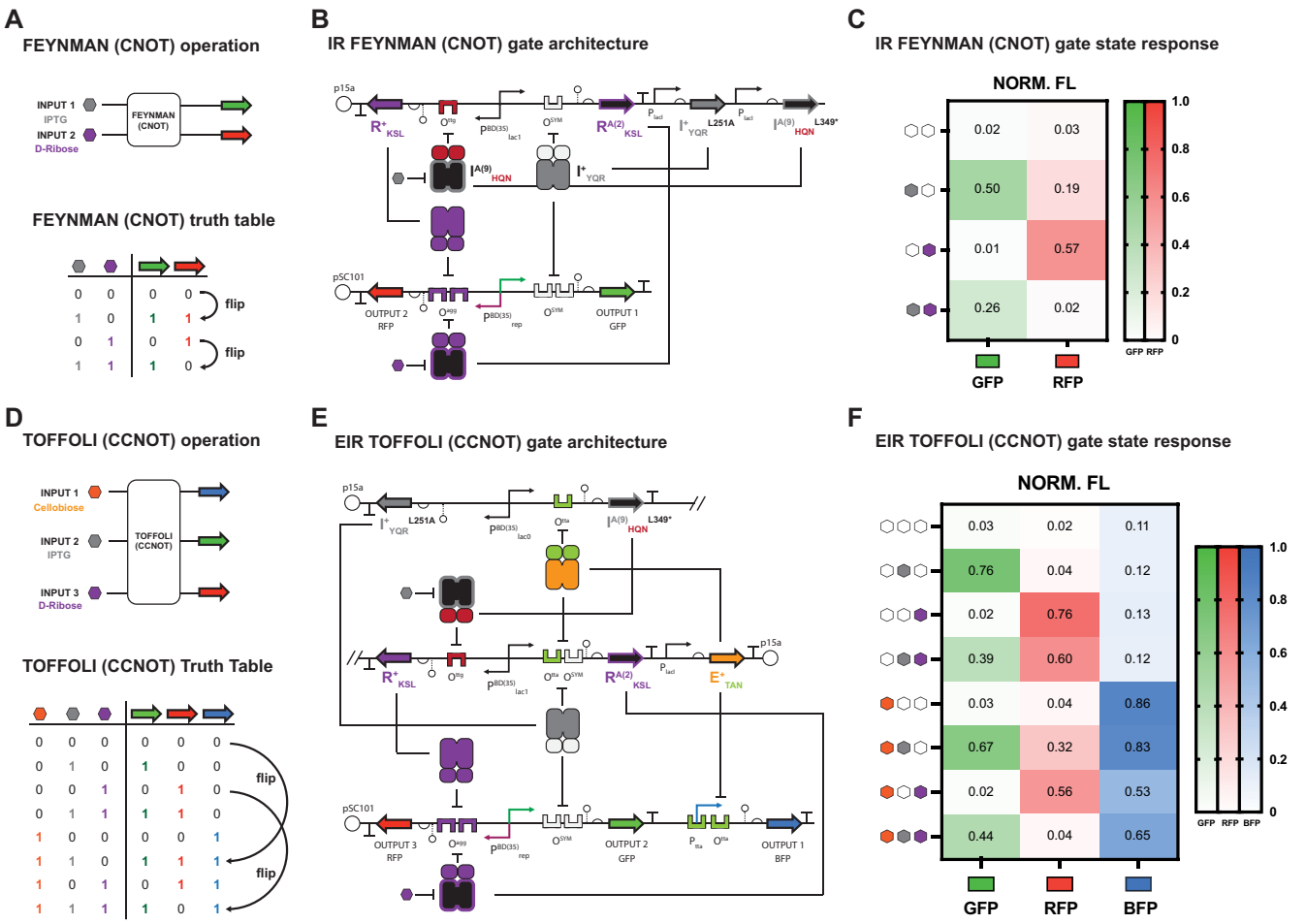

Figure 4. Biological FEYNMAN and TOFFOLI logic gates. (**A**) Biological IPTG–D-ribose FEYNMAN logic gate diagram and truth table. The OUTPUT state is flipped when INPUT 1 (IPTG) is present. (**B**) Genetic architecture of IR FEYNMAN logic gate. IPTG-inducible transcription factors I^{+}_{YQR} L251A and $I^{A(9)}_{HQN}$ L349* regulate a D-ribose-inducible transcription factor layer comprised of R^{+}_{KSL} and $R^{A(2)}_{KSL}$ driven by the $P^{BD(35)}_{lac1}$ bidirectional promoter. Regulated D-ribose transcription factors FEEDFORWARD to regulate the 2-OUTPUT $P^{BD(35)}_{rep}$ reporter. (**C**) Performance of IR FEYNMAN logic gate. INPUT conditions (rows) and OUTPUT expression (columns) are shown for GFP and RFP . Numerical values represent the OUTPUT measurement on a fractional scale (Methods). (**D**) Biological cellobiose–IPTG–D-ribose (EIR) TOFFOLI logic gate diagram and truth table. The OUTPUT state is flipped when both INPUT 1 (cellobiose) and INPUT 2 (IPTG) are present. (**E**) Genetic architecture of EIR TOFFOLI logic gate. The cellobiose-inducible repressor E^{+}_{TAN} regulates both $I^{A(9)}_{HQN}$ L349* and $R^{A(2)}_{KSL}$ anti-repressors, as well as a BFP (control) OUTPUT on the reporter. Regulated $I^{A(9)}_{HQN}$ L349* and I^{+}_{YQR} L251A regulate R^{+}_{KSL} and $R^{A(2)}_{KSL}$, respectively, which FEEDFORWARD to regulate GFP and RFP. The $P^{BD(35)}_{lac0}$ and $P^{BD(35)}_{lac1}$ bidirectional promoters drive transcription of IPTG-inducible transcription factors I^{+}_{YQR} L251A and $I^{A(9)}_{HQN}$ L349*, and D-ribose-inducible transcription factors R^{+}_{KSL} and $R^{A(2)}_{YQR}$, respectively. (**F**) Performance of EIR TOFFOLI logic gate. INPUT conditions (rows) and OUTPUT expression (columns) are shown for GFP, RFP, and BFP.

permutation space (Fig. 5A and B). The design is predicated on a single layer containing two QUBIT operations, coordinating two sets of synthetic transcription factors, such that each set responds to a different INPUT signal—i.e. IPTG or D-ribose (Fig. 5C). Notably, each synthetic transcription factor utilizes an orthogonal DNA-binding function. The given bi-QUBIT architecture coordinates the expression of four disparate OUTPUT reporters via sets of orthogonal tandem operator pairs. To accomplish this, we redesigned the D-ribose QUBIT to accommodate additional DNA-binding functions—i.e. via operators O^{gta} and O^{ttg} (see Supplementary Fig. S15). Once we validated the new binding operation, we constructed the final bi-QUBIT system—where QUBIT 1 is mapped to the regulation of YFP or GFP and QUBIT 2 is mapped to regulate BFP or RFP, circuit design given in Fig. 5C. Finally, we tested the 2-QUBIT 4-OUTPUT circuit, which was faithful to the design goal—i.e. each INPUT set mapped to a unique OUTPUT—see Fig. 5D and Supplementary Fig. S16.

Engineering quantum swap-of-function memory operations

Genetic memory operations use recombinases to invert or excise genetic elements, which facilitate permanent changes to DNA that are inheritable [26, 52–54] (see Fig. 6A). A hallmark of synthetic biological intelligence is the integration of decision-making programs with recombinase-based memory operations [43, 44]. Said memory operations can be broadly classified as gain-of-function (GoF) or loss-of-function unit operations. We posited that we could leverage the bidirectional synthetic promoters and genetic programming structure developed in this work to engineer a third memory operation in the form of swap-of-function (SoF), between two fundamental reversible logic operations (see Fig. 6B).

We posited that we could engineer an invertible synthetic promoter capable of directing two disparate synthetic transcription factors, such that said element could be prompted to remap OUTPUT regulation *in situ*. To accomplish this, we

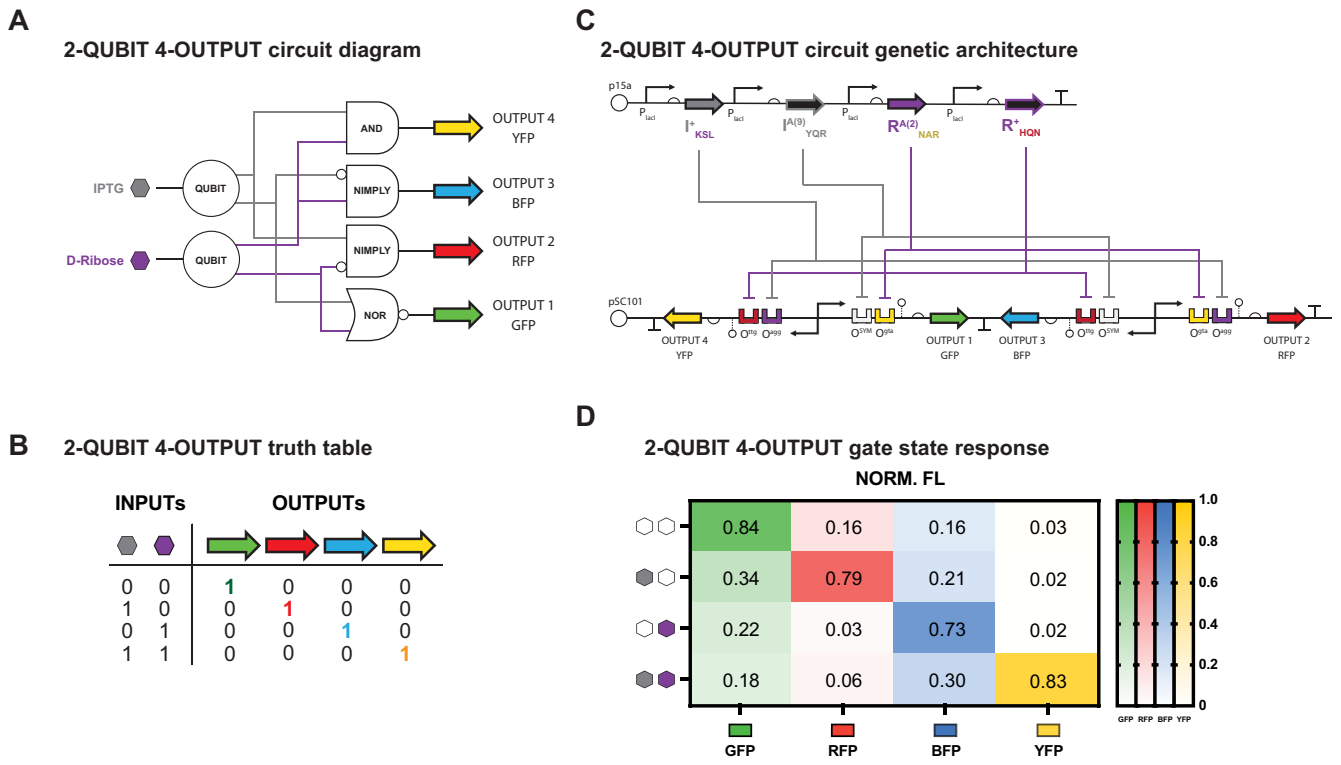

Figure 5. Engineered 4-OUTPUT circuit using biological QUBIT gates. (**A**) Diagram of 4-OUTPUT circuit. IPTG and D-ribose QUBIT gates are used to regulate four fluorescent reporter OUTPUTs—GFP, RFP, BFP, and YFP—with NOR, A NIMPLY B, B NIMPLY A, or AND logic, respectively. (**B**) Truth table and (**C**) genetic architecture of 4-OUTPUT circuit. IPTG QUBIT gate transcription factors I^{+}_{KSL} L251A and $I^{A(9)}_{YQR}$ L349* and D-ribose QUBIT gate transcription factors $R^{A(2)}_{NAR}$ and R^{+}_{HQN} are constitutively expressed and regulate each of the four OUTPUTs on the reporter. Each OUTPUT is expressed from $P^{BD(35)}_{rep}$ bidirectional promoters analogous to the QUBIT architectures shown previously, with the modification of orthogonal operator combinations upstream of each OUTPUT. This modification allows for the full development of the abstract logic gate scheme showed in panel (A), and corresponding truth table given in panel (B). (**D**) Performance of 4-OUTPUT circuit. The fluorescence of each OUTPUT is indicated for each INPUT combination. Mean values are normalized to a scale of 1 for each OUTPUT and displayed on the plot—see the "Materials and methods" section for details.

used the transcription factor PhlF [2, 55] to regulate the serine recombinase A118 [56], which interacts with a set of anti-aligned attachment sites (*attB* and *attP*—i.e. oriented to facilitate inversion) flanking the operator sequences of a given bidirectional synthetic promoter (Fig. 6C). In principle, induction of PhlF prompts the expression of recombinase A118, which catalyzes the inversion of the bidirectional promoter and operator sequences. Said recombination event effectively swaps the regulatory control of GFP and RFP OUTPUT channels—i.e. we can induce the transformation of a biological QUBIT gate to a PAULI-X gate via a SoF memory operation.

We built and tested two iterations of the said SoF (QUBIT to PAULI-X) memory operation—(i) one unit operation responsive to IPTG and (ii) another responsive to D-ribose (Fig. 6D and E, and Supplementary Fig. S17). In both cases, the SoF memory operation performed as expected observed by flow cytometry (also see Supplementary Figs S6 and S18). This result demonstrates the successful convergence of memory with reversible logic, introducing the ability to engineer intelligent biological systems with expanded functionality and greater dynamic programming capabilities.

Discussion

In this study, we present a novel toolkit for constructing next-generation synthetic biological decision-making with advanced INPUT economy predicated on reversible logic—i.e. biological QUBIT operations that can be used as building blocks. The modular nature of said technology builds on our T-Pro platform via leveraging previously developed synthetic transcription factors paired with novel bidirectional synthetic promoters developed in this study. Layering of biological QUBITs allows for the systematic expansion of reversible programs from 1-INPUT, 2-OUTPUT operations to more advanced multiple-INPUT, multiple-OUTPUT reversible logical operations. Commensurate with the tenets of intelligent biological systems, our quantum-inspired technology can be systematically paired with memory operations to form SoF units of inheritable function. Additionally, the use of bidirectional synthetic promoters allows for additional circuit compression—i.e. inherent (and complementary) to our original T-Pro toolkit—via consolidating transcription initiation of two disparate OUTPUTs to a single event.

Our quantum-inspired platform for decision-making marks a clear advance over current reversible gate technology in a single chassis cell [42]. Namely, the state of the art prior to this study demonstrated and is limited to an apparent FEYNMAN operation (see Supplementary Fig. S14D), which poses a limit to scalability and biocomputing capability. In contrast, our platform technology developed in this study is predicated on fundamental QUBIT building blocks that are scalable and resource efficient (i.e. compressed) enabling unprecedented biocomputing capability and capacity in a single chassis cell. Barring resource limits of the chassis cell, a key limitation of our quantum-inspired wetware is the number of orthogonal synthetic transcription factors available for INPUT processing. Our current design space for synthetic

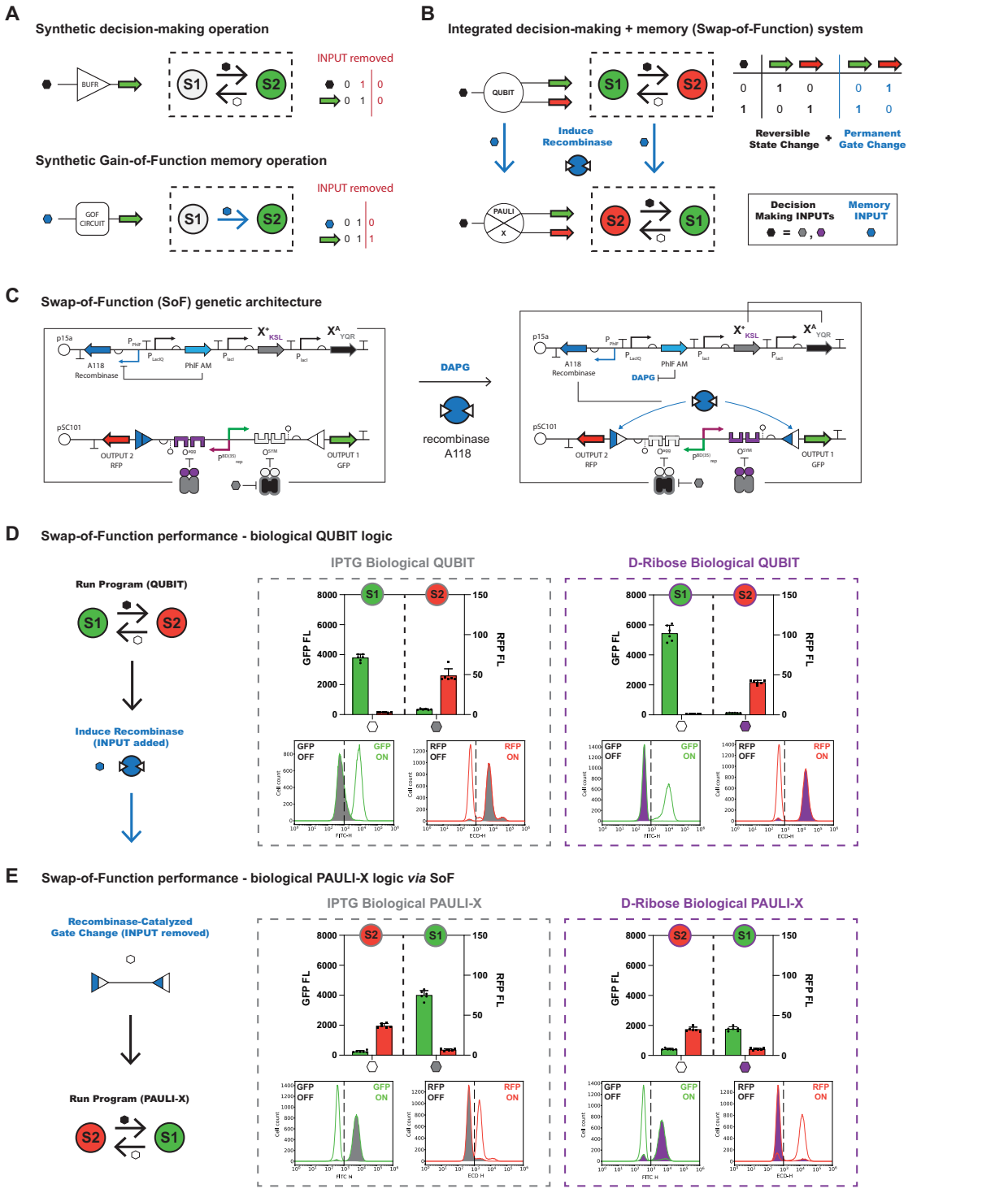

Figure 6. Recombinase-based QUBIT to PAULI-X gate SoF memory operation. (**A**) Example of a conventional decision-making only system comprised of a single logical BUFFER operation. When the INPUT (hexagon) is added or removed, the OUTPUT state reversibly changes from ON to OFF, respectively. Example of a recombinase-mediated memory only system composed of a single GoF operation. When the INPUT (hexagon) is added to the system, the OUTPUT state permanently changes from OFF to ON via DNA recombination. (**B**) Diagram of QUBIT to PAULI-X gate conversion operation that offers cooperative decision-making and memory functions. A biological QUBIT gate, which performs reversible OUTPUT state change (i.e. GFP to RFP) upon addition of the decision-making INPUT, is transformed to a PAULI-X gate via the addition of a memory INPUT. The resulting PAULI-X gate performs the reverse OUTPUT state change (i.e. RFP to GFP) upon addition of the decision-making INPUT. (**C**) Genetic architecture of QUBIT to PAULI-X gate conversion memory operation. The transcription factor PhlF is expressed constitutively and regulates the recombinase A118. Additionally, a repressor (X^{+}_{KSL}) and anti-repressor (X^{A}_{YQR}) regulates—i.e. X = I or R—the $P^{BD(35)}_{rep}$ inducible promoter flanked by A118 recombinase *attB* and *attP* attachment sites. Upon PhlF induction (with DAPG), A118 is produced and inverts the $P^{BD(35)}_{rep}$ promoter and operator DNA element, inverting the regulatory control of each OUTPUT and converting the biological QUBIT gate to a biological PAULI-X gate. (**D**) Performance of IPTG and D-ribose biological QUBIT gates. Each OUTPUT was measured with plate reader (bars) and flow cytometry (histograms) (see the "Materials and methods" section). Following measurements, the memory operation was performed, and the circuits were re-assayed with the same conditions. (**E**) Memory of biological PAULI-X logic (converted QUBIT gates) as described in panel (D).

transcription factors is on the order of 10^8 with over 1000 putatively orthogonal INPUTs; in addition, said T-Pro biosensing functions can be expanded via established protein engineering workflows [57]. Accordingly, we posit that our wetware has the potential of becoming a complete programming language. We note that the objective of biocomputing is not to displace abiotic computing—i.e. *in silico* and the like—rather the goal is to leverage biocomputing to confer decision-making and synthetic intelligence in biological systems for next-generation biomanufacturing, living therapeutics, and similar biotechnologies.

Another limitation of our platform technology is biological circuit designs optimized for compression. Namely, as circuit complexity increases with higher-state computation, the design of the most compressed iteration of desired circuits cannot be guaranteed without additional optimization (software) strategies. In any case, we believe that this is a tractable problem and clearly marks the next objective for our platform technology. Taken together, this study represents a paradigm shift in synthetic biology decision-making enabling the expansion of T-Pro from Boolean logical operations to quantum-inspired logical operations. We posit that said platform technology will be of use in myriad applications that utilize both coding and noncoding RNA and combinations thereof.

Acknowledgements

Author contributions: Prasaad T. Milner (Conceptualization [equal], Data curation [equal], Formal analysis [equal], Methodology [equal], Writing—original draft [equal], Writing—review & editing [supporting]), Dowan Kim (Conceptualization [supporting], Data curation [supporting], Formal analysis [supporting], Methodology [supporting]), and Corey J. Wilson (Conceptualization [lead], Formal analysis [equal], Funding acquisition [lead], Investigation [equal], Methodology [equal], Project administration [lead], Supervision [lead], Validation [lead], Writing—original draft [equal], Writing—review & editing [lead]).

Supplementary data

Supplementary data is available at NAR online.

Conflict of interest

None declared.

Funding

This work was supported by National Science Foundation grant numbers 1934836, 2123855, 2226663, and 2319231, and the National Institutes of Health grant number R35GM153457 (all awarded to C.J.W.). Funding to pay the Open Access publication charges for this article was provided by National Science Foundation grant number 2123855.

Data availability

All data collected in this study are provided in the Supplementary data and related source data files. Source data are provided with this paper. Plasmid sequences are available from GenBank with accession numbers PQ511351–PQ511377. Materials generated in this study are available upon request.

References

1. Guet CC, Elowitz MB, Hsing WH *et al.* Combinatorial synthesis of genetic networks. *Science* 2002;**296**:1466–70. https://doi.org/10.1126/science.1067407
2. Meyer AJ, Segall-Shapiro TH, Glassey E *et al. Escherichiacoli* "Marionette" strains with 12 highly optimized small-molecule sensors. *Nat Chem Biol* 2019;**15**:196–204. https://doi.org/10.1038/s41589-018-0168-3
3. Chen Y, Zhang SY, Young EM *et al.* Genetic circuit design automation for yeast. *Nat Microbiol* 2020;**5**:1349–60. https://doi.org/10.1038/s41564-020-0757-2
4. Taketani M, Zhang J, Zhang S *et al.* Genetic circuit design automation for the gut resident species *Bacteroides thetaiotaomicron*. *Nat Biotechnol* 2020;**38**:962–9. https://doi.org/10.1038/s41587-020-0468-5
5. Nielsen AA, Der BS, Shin J *et al.* Genetic circuit design automation. *Science* 2016;**352**:aac7341. https://doi.org/10.1126/science.aac7341
6. Ausländer D, Ausländer S, Pierrat X *et al.* Programmable full-adder computations in communicating three-dimensional cell cultures. *Nat Methods* 2018;**15**:57–60.https://doi.org/10.1038/nmeth.4505
7. Zhou Z, Liu Y, Feng Y *et al.* Engineering longevity—design of a synthetic gene oscillator to slow cellular aging. *Science* 2023;**380**:376–81. https://doi.org/10.1126/science.add7631
8. Wu Y, Li Y, Jin K *et al.* CRISPR-dCas12a-mediated genetic circuit cascades for multiplexed pathway optimization. *Nat Chem Biol* 2023;**19**:367–77. https://doi.org/10.1038/s41589-022-01230-0
9. Rondon RE, Groseclose TM, Short AE *et al.* Transcriptional programming using engineered systems of transcription factors and genetic architectures. *Nat Commun* 2019;**10**:4784. https://doi.org/10.1038/s41467-019-12706-4
10. Groseclose TM, Rondon RE, Herde ZD *et al.* Engineered systems of inducible anti-repressors for the next generation of biological programming. *Nat Commun* 2020;**11**. 4440 https://doi.org/10.1038/s41467-020-18302-1
11. Milner PT, Zhang ZQ, Herde ZD *et al.* Performance prediction of fundamental transcriptional programs. *ACS Synth Biol* 2023;**12**:1094–108. https://doi.org/10.1021/acssynbio.2c00593
12. Shin J, Zhang S, Der BS *et al.* Programming *Escherichia coli* to function as a digital display. *Mol Syst Biol* 2020;**16**:e9401. https://doi.org/10.15252/msb.20199401
13. Huang BD, Groseclose TM, Wilson CJ. Transcriptional programming in a *Bacteroides* consortium. *Nat Commun* 2022;**13**:3901. https://doi.org/10.1038/s41467-022-31614-8
14. Zhu R, Del Rio-Salgado JM, Garcia-Ojalvo J *et al.* Synthetic multistability in mammalian cells. *Science* 2022;**375**:eabg9765. https://doi.org/10.1126/science.abg9765
15. Park JH, Bassalo MC, Lin GM *et al.* Design of four small-molecule-inducible systems in the yeast chromosome, applied to optimize terpene biosynthesis. *ACS Synth Biol* 2023;**12**:1119–32. https://doi.org/10.1021/acssynbio.2c00607
16. Zhang F, Carothers JM, Keasling JD. Design of a dynamic sensor-regulator system for production of chemicals and fuels derived from fatty acids. *Nat Biotechnol* 2012;**30**:354–9. https://doi.org/10.1038/nbt.2149
17. Mannan AA, Bates DG. Designing an irreversible metabolic switch for scalable induction of microbial chemical production. *Nat Commun* 2021;**12**:3419. https://doi.org/10.1038/s41467-021-23606-x
18. Xu X, Li X, Liu Y *et al.* Pyruvate-responsive genetic circuits for dynamic control of central metabolism. *Nat Chem Biol* 2020;**16**:1261–8. https://doi.org/10.1038/s41589-020-0637-3
19. Moser F, Espah Borujeni A, Ghodasara AN *et al.* Dynamic control of endogenous metabolism with combinatorial logic circuits. *Mol Syst Biol* 2018;**14**:e8605. https://doi.org/10.15252/msb.20188605
20. Kang CW, Lim HG, Won J *et al.* Circuit-guided population acclimation of a synthetic microbial consortium for improved biochemical production. *Nat Commun* 2022;**13**:6506. https://doi.org/10.1038/s41467-022-34190-z

21. Chan CTY, Lee JW, Cameron DE *et al.* 'Deadman' and 'Passcode' microbial kill switches for bacterial containment. *Nat Chem Biol* 2016;**12**:82–6. https://doi.org/10.1038/nchembio.1979
22. Stirling F, Bitzan L, O'Keefe S *et al.* Rational design of evolutionarily stable microbial kill switches. *Mol Cell* 2017;**68**:686–97.e3. https://doi.org/10.1016/j.molcel.2017.10.033
23. Xue YB, Du P, Shendi AAI *et al.* Mercury bioremediation in aquatic environment by genetically modified bacteria with self-controlled biosecurity circuit. *J Cleaner Prod* 2022;**337**:130524. https://doi.org/10.1016/j.jclepro.2022.130524
24. Brophy JAN, Magallon KJ, Duan L *et al.* Synthetic genetic circuits as a means of reprogramming plant roots. *Science* 2022;**377**:747–51. https://doi.org/10.1126/science.abo4326
25. Ryu MH, Zhang J, Toth T *et al.* Control of nitrogen fixation in bacteria that associate with cereals. *Nat Microbiol* 2020;**5**:314–30. https://doi.org/10.1038/s41564-019-0631-2
26. Lloyd JPB, Ly F, Gong P *et al.* Synthetic memory circuits for stable cell reprogramming in plants. *Nat Biotechnol* 2022;**40**:1862–72. https://doi.org/10.1038/s41587-022-01383-2
27. Triassi AJ, Fields BD, Monahan CE *et al.* Redesign of an *Escherichia coli* Nissle treatment for phenylketonuria using insulated genomic landing pads and genetic circuits to reduce burden. *Cell Syst* 2023;**14**:512–24. https://doi.org/10.1016/j.cels.2023.05.004
28. Abedi MH, Yao MS, Mittelstein DR *et al.* Ultrasound-controllable engineered bacteria for cancer immunotherapy. *Nat Commun* 2022;**13**:1585. https://doi.org/10.1038/s41467-022-29065-2
29. Deng F, Pan J, Liu Z *et al.* Programmable DNA biocomputing circuits for rapid and intelligent screening of SARS-CoV-2 variants. *Biosens Bioelectron* 2023;**223**:115025. https://doi.org/10.1016/j.bios.2022.115025
30. Li HS, Israni DV, Gagnon KA *et al.* Multidimensional control of therapeutic human cell function with synthetic gene circuits. *Science* 2022;**378**:1227–34. https://doi.org/10.1126/science.ade0156
31. Xie M, Fussenegger M. Designing cell function: assembly of synthetic gene circuits for cell biology applications. *Nat Rev Mol Cell Biol* 2018;**19**:507–25. https://doi.org/10.1038/s41580-018-0024-z
32. Grozinger L, Amos M, Gorochowski TE *et al.* Pathways to cellular supremacy in biocomputing. *Nat Commun* 2019;**10**: 5250. https://doi.org/10.1038/s41467-019-13232-z
33. Thapliyal H, Ranganathan N. Design of reversible sequential circuits optimizing quantum cost, delay, and garbage outputs. *J Emerg Technol Comput Syst* 2010;**6**:1–31. https://doi.org/10.1145/1877745.1877748
34. Peres A. Reversible logic and quantum computers. *Phys Rev A* 1985;**32**:3266–76. https://doi.org/10.1103/PhysRevA.32.3266
35. Takeuchi N, Yamanashi Y, Yoshikawa N. Reversible logic gate using adiabatic superconducting devices. *Sci Rep* 2014;**4**:6354. https://doi.org/10.1038/srep06354
36. Rao DGS, Swarnakar S, Kumar S. Design of all-optical reversible logic gates using photonic crystal waveguides for optical computing and photonic integrated circuits. *Appl Opt* 2020;**59**:11003–12. https://doi.org/10.1364/AO.409404
37. Choudhary K, Kumar S. Optimized plasmonic reversible logic gate for low loss communication. *Appl Opt* 2021;**60**:4567–72. https://doi.org/10.1364/AO.428158
38. Orbach R, Remacle F, Levine RD *et al.* Logic reversibility and thermodynamic irreversibility demonstrated by DNAzyme-based Toffoli and Fredkin logic gates. *Proc Natl Acad Sci USA* 2012;**109**:21228–33. https://doi.org/10.1073/pnas.1219672110
39. Fratto BE, Katz E. Controlled logic gates—switch gate and Fredkin gate based on enzyme-biocatalyzed reactions realized in flow cells. *ChemPhysChem* 2016;**17**:1046–53. https://doi.org/10.1002/cphc.201501095
40. Sarkar K, Bonnerjee D, Srivastava R *et al.* A single layer artificial neural network type architecture with molecular engineered bacteria for reversible and irreversible computing. *Chem Sci* 2021;**12**:15821–32. https://doi.org/10.1039/D1SC01505B
41. Srivastava R, Bagh S. A logically reversible double Feynman gate with molecular engineered bacteria arranged in an artificial neural network-type architecture. *ACS Synth Biol* 2023;**12**:51–60. https://doi.org/10.1021/acssynbio.2c00520
42. Srivastava R, Sarkar K, Bonnerjee D *et al.* Synthetic genetic reversible Feynman gate in a single *E. coli* cell and its application in bacterial to mammalian cell information transfer. *ACS Synth Biol* 2022;**11**:1040–8. https://doi.org/10.1021/acssynbio.1c00392
43. Short AE, Kim D, Milner PT *et al.* Next generation synthetic memory via intercepting recombinase function. *Nat Commun* 2023;**14**:5255. https://doi.org/10.1038/s41467-023-41043-w
44. Huang BD, Kim D, Yu Y *et al.* Engineering intelligent chassis cells via recombinase-based MEMORY circuits. *Nat Commun* 2024;**15**:2418. https://doi.org/10.1038/s41467-024-46755-1
45. Rondon RE, Wilson CJ. Engineering a new class of anti-LacI transcription factors with alternate DNA recognition. *ACS Synth Biol* 2019;**8**:307–17. https://doi.org/10.1021/acssynbio.8b00324
46. Warman EA, Forrest D, Guest T *et al.* Widespread divergent transcription from bacterial and archaeal promoters is a consequence of DNA-sequence symmetry. *Nat Microbiol* 2021;**6**:746–56. https://doi.org/10.1038/s41564-021-00898-9
47. Davey JA, Wilson CJ. Engineered signal-coupled inducible promoters: measuring the apparent RNA-polymerase resource budget. *Nucleic Acids Res* 2020;**48**:9995–10012. https://doi.org/10.1093/nar/gkaa734
48. Dong F, Spott S, Zimmermann O *et al.* Dimerisation mutants of Lac repressor. I. A monomeric mutant, L251A, that binds Lac operator DNA as a dimer. *J Mol Biol* 1999;**290**:653–66. https://doi.org/10.1006/jmbi.1999.2902
49. Chen J, Matthews KS. Deletion of lactose repressor carboxyl-terminal domain affects tetramer formation. *J Biol Chem* 1992;**267**:13843–50. https://doi.org/10.1016/S0021-9258(19)49645-2
50. Marinescu DC, Marinescu GM. *Classical and Quantum Information*. Burlington, MA: Academic Press, 2012.
51. Fedorov A, Steffen L, Baur M *et al.* Implementation of a Toffoli gate with superconducting circuits. *Nature* 2012;**481**:170–2. https://doi.org/10.1038/nature10713
52. Siuti P, Yazbek J, Lu TK. Synthetic circuits integrating logic and memory in living cells. *Nat Biotechnol* 2013;**31**:448–52. https://doi.org/10.1038/nbt.2510
53. Yang L, Nielsen AA, Fernandez-Rodriguez J *et al.* Permanent genetic memory with >1-byte capacity. *Nat Methods* 2014;**11**:1261–6.
54. Guiziou S, Mayonove P, Bonnet J. Hierarchical composition of reliable recombinase logic devices. *Nat Commun* 2019;**10**:456. https://doi.org/10.1038/s41467-019-08391-y
55. Stanton BC, Nielsen AAK, Tamsir A *et al.* Genomic mining of prokaryotic repressors for orthogonal logic gates. *Nat Chem Biol* 2014;**10**:99–105. https://doi.org/10.1038/nchembio.1411
56. Loessner MJ, Inman RB, Lauer P *et al.* Complete nucleotide sequence, molecular analysis and genome structure of bacteriophage A118 of *Listeria monocytogenes*: implications for phage evolution. *Mol Microbiol* 2000;**35**:324–40. https://doi.org/10.1046/j.1365-2958.2000.01720.x
57. Hersey AN, Kay VE, Lee S *et al.* Engineering allosteric transcription factors guided by the LacI topology. *Cell Syst* 2023;**14**:645–55. https://doi.org/10.1016/j.cels.2023.04.008
58. Tomasello G, Armenia I, Molla G. The Protein Imager: a full-featured online molecular viewer interface with server-side HQ-rendering capabilities. *Bioinformatics* 2020;**36**:2909–11. https://doi.org/10.1093/bioinformatics/btaa009

Received: October 14, 2024. **Revised:** April 27, 2025. **Editorial Decision:** May 3, 2025. **Accepted:** May 12, 2025